A Study of Impeller-Diffuser-Volute Interaction in a Centrifugal Fan

Tarek Meakhail
e-mail: mina_tarek@hotmail.com

Seung O. Park
e-mail: sopark@sop1.kaist.ac.kr

Korea Advanced Institute of Science and Technology,
Yuseong-gu,
Daejeon 305-701, Korea

This paper reports velocity measurement data in the interaction region between the impeller and vaned diffuser and the results of numerical flow simulation of the whole machine (impeller, vaned diffuser and volute) of a single stage centrifugal fan. Two-dimensional instantaneous velocity measurement is done using particle image velocimetry (PIV). Numerical simulation of impeller-diffuser-volute interaction is performed using CFX-Tascflow commercial code. A frozen rotor simulation model is used for the steady calculation and a rotor-stator simulation model is used for the unsteady calculation using the steady results as an initial guess. The simulation results show that the separated flow regime near the diffuser hub extends to the volute. Comparison between the unsteady computation and those of measurement indicates that the rotor/stator model employed in the simulation predicts essential characteristics of unsteady flow in the centrifugal fan. However, quantitative agreement remains rather poor. [DOI: 10.1115/1.1812318]

Introduction

There has been steady progress in the field of turbomachinery flow computations during the past decade. These advances have made it possible for turbomachinery designers to carry out analysis of various flow phenomena occurring inside turbomachines. To improve design of centrifugal machines, a better understanding of the flow of such machines is required. This paper deals with an experimental and theoretical study of the flow in a low specific-speed centrifugal fan.

A number of authors have treated the problem of the interaction of the impeller and its surroundings numerically and experimentally. Inoue and Cumpsty [1], Sideris and Braembussche [2] and Arndt et al. [3,4] have been concerned with the action of the diffuser. Paone et al. [5] at VKI have used particle image displacement velocimetry (PIDV) to measure the flow field inside the vaneless diffuser of a centrifugal pump made of plexiglass with a shrouded impeller. They compared the PIDV measurements and the corresponding LDV measurement data and found that they were different in the wake. They believed that the information available from PIDV could largely contribute to a better understanding of the flow in centrifugal machines. Also, at VKI, Hillewaert and Van den Braembussche [6] have studied numerically the problem of impeller-volute interaction in a centrifugal compressor. So far, the measurement of the instantaneous whole flow field in the interaction region between the impeller and the diffuser or numerical simulation of the whole machine could not be found in the literature. The purpose of this paper is to introduce a numerical simulation of the whole machine and to compare the numerical results to those obtained by PIV measurement at the interaction region between the impeller and the diffuser at different relative location.

The Centrifugal Fan

Figure 1 shows a single stage centrifugal fan made of plexiglass. It consists of impeller, diffuser (vaned or vaneless) and volute. More details of the test rig, performance and PIV measurement data can be found in Meakhail et al. [7,8]. Steady and unsteady numerical simulation of the whole fan is performed using CFX-Tascflow commercial Code, using a HP-Unix workstation. A ''frozen rotor'' simulation is used first to find the preliminary steady flow field. A ''rotor-stator'' simulation is used to find final unsteady flow, using the steady results as an initial guess.

Numerical Technique

The commercially available CFD code, CFX-Tascflow [9], is employed for this study. The validation of this code for the turbomachinery flows can be found, for example, in the work of Gernot et al. [10], Peter and Donald [11] and Mihael et al. [12]. The code solves the Reynolds averaged Navier–Stokes equations in primitive variable form. The effects of turbulence were modeled using the standard K-ε turbulence model. To make the simulation time economical, wall function is used to resolve the wall flows.

Grid Generation

A high quality mesh is produced using a single block H-grid through the main blade and the passage (for both impeller and diffuser) using CFX-Turbogrid software [13]. CFX-Tascgrid is used for volute grid generation. This type of grid generation gives better minimum skew angle, which should not be less than 20 deg, and better maximum aspect ratio, which should not be more than 100. The blades are defined by blocking off grid elements. The entire grid size for one blade is

For the impeller		
Entire grid:	42*32*23=30,912	(I, J, K)
Blade block off	24*8*23=4416	(I, J, K)
For the vaned diffuser		
Entire grid:	46*27*23=28,566	(I, J, K)
Blade block off	22*5*23=2530	(I, J, K)

For the volute, the grid consists of several blocks and the total number of nodes is 230,000 nodes

Figure 2 shows the grid system of the present calculation. The total number of grid nodes is around 1,000,000 nodes for the whole impeller, diffuser and volute.

Transient Rotor/Stator and Frozen-Rotor Simulation

The frozen rotor simulation is used to get the steady state solution for different components of the machine. That is, the interface condition is in steady state and the geometry remain fixed across the interface.

Contributed by the International Gas Turbine Institute (IGTI) of THE AMERICAN SOCIETY OF MECHANICAL ENGINEERS for publication in the ASME JOURNAL OF TURBOMACHINERY. Paper presented at the International Gas Turbine and Aeroengine Congress and Exhibition, Vienna, Austria, June 13–17, 2004, Paper No. 2004-GT-53068. Manuscript received by IGTI, October 1, 2003; final revision, March 1, 2004. IGTI Review Chair: A. J. Strazisar.

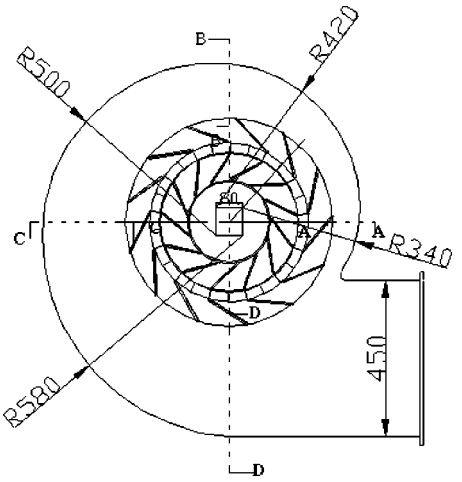

Fig. 1 The centrifugal fan

A transient rotor/stator simulation can be used any time when it is desired to account for transient interaction effects at a sliding (frame change) interface. By nature, these simulations are always transient, never achieving a steady state condition. The components on each side of a transient sliding interface are always in relative motion with respect to each other. Pitch change is automatically dealt with at a transient sliding interface in the same manner as at frozen rotor interfaces: the profiles in the pitch-wise direction are stretched or compressed to the extent that there is pitch change across the interface. As with the frozen rotor condition, the computational accuracy degrades rapidly with increasing pitch change.

Boundary Conditions

There are several different types of boundary condition that can be applied at the inlet boundary. For example, the velocity (or mass flow rate) can be specified or total pressure can be specified.

The velocity is specified over the entire inlet face of the impeller for most computational cases. The average inlet velocity is 5 m/s at the outlet, the measured static pressure applied as an average value over the outlet area of the volute ($P_{out}=102{,}200$ Pa). However, for the computations to evaluate performance parameter, total pressure is applied at the inlet. The diffuser and volute are stationary and the impeller is rotating with a rotational speed of 1000 rev/min. A sliding interface model is set between the impeller and diffuser. Additionally, the K-ε turbulence model in Tascflow requires an inlet value for the turbulence intensity (Tu) and the eddy length (L), which can be calculated as the cubic root of the volume of the calculation domain. The computations for the present work run in fully turbulent mode with Tu$=5\%$ and $L=0.5$ and the Reynolds number is 4.5E4.

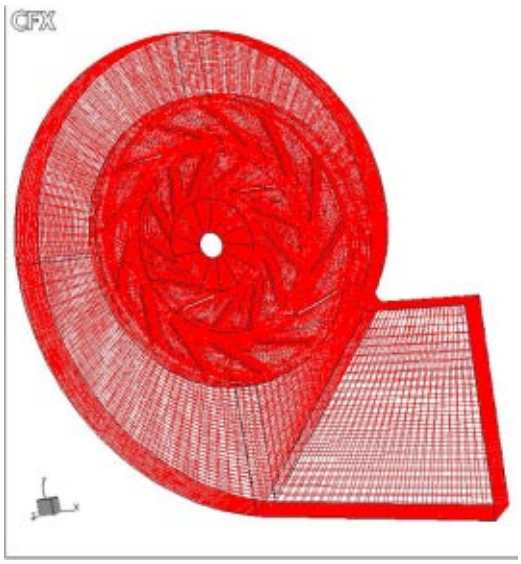

Fig. 2 The grid system

Solution Procedures

The frozen rotor simulation is obtained first using a larger time step ($\Delta t=1E-3$ s). The transient simulation is done using a smaller time step ($\Delta t=1.5E-4$ s) with using the frozen rotor simulation as an initial guess. The number of iteration per time step is 10. The calculation results discussed here were run on HP-UNIX workstation with 512 Mbytes of memory, which can be extended to a virtual memory of 1Gbyte. Typical CPU times were around 2 days for 200 iterations for frozen rotor simulation and 5 days for 60 time steps for transient simulation necessary for a run to converge down to maximum residuals of less than $E-04$.

Results and Discussion

Frozen Rotor Simulation. The flow leaving the rotating impeller is very complex and presents nonuniformities between the hub and the shroud as well as in the circumferential direction. These nonuniformities result from the secondary flow that develops in the machines. Under the action of the centrifugal and Coriolis forces low momentum fluid accumulates in the shroud-suction side corner. This migration of the low momentum fluid led to the so-called *jet-wake* model. This model was very popular in the past, but as detailed measurements became available, it appears that the model is too idealized. Therefore, in view of the complexity of the outflow, it appears doubtful that a simple model can be used to construct the flow entering the downstream blade row, making the uncoupled unsteady approach not practical for designing any new rotating machine. Also, it must be pointed out here that the jet/wake structure is a complicated flow phenomenon. Each impeller has its own jet/wake structure. For example, Eckardt [14] has found the wake region near the shroud suction side, while Kirtley and Beach [15] have found the wake region near the shroud pressure side. Hamkins and Flack [16] showed a migration of vortex from suction side to the pressure side. On the other hand, Krain and Hoffman [17] found that there was no jet/wake characteristics at all but the flow went smoothly at the impeller exit.

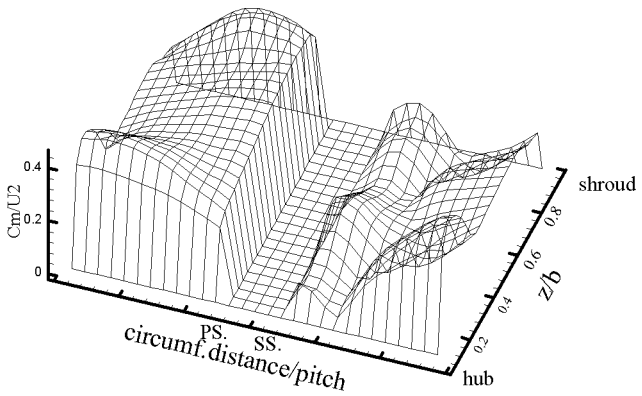

Fig. 3 Normalized meridional velocity profile at the exit plane of the impeller

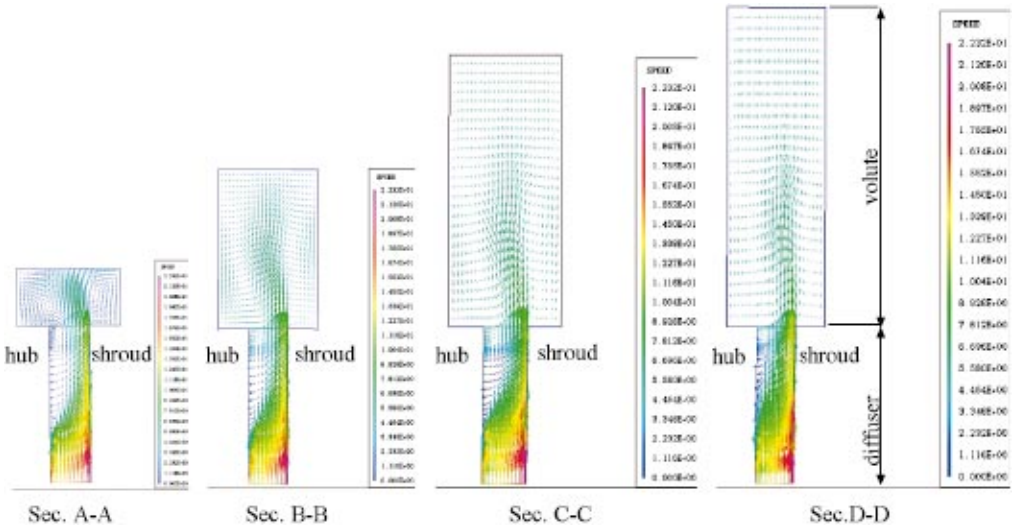

Fig. 4 Velocity vectors at design flow rate for diffuser and volute at different sections

The predicted impeller flow exhibits a jet/wake structure. Figure 3 shows a relief plot of the steady state-predicted meridional flow velocity normalized by impeller tip speed (C_{mer}/U_2) at the exit plane of the impeller at medium flow rate. C_{mer} is calculated from the equation:

$$C_{mer} = \sqrt{C_{rad}^2 + C_{tan}^2 + C_{ax}^2}$$

The figure shows a clear jet-like flow (of high meridional flow velocity) at the pressure side and a wake-like flow (of lower velocity) near the hub suction side. Apart from this low velocity region near the hub, another low velocity region around $z/b = 0.7$ is also found.

Figure 4 shows the velocity vectors in the meridional plane, sections A-A, B-B, C-C and D-D for vaned diffuser and volute at best efficiency point (BEP), close to the design point. The figure shows a detached flow region in the hub side starting at a location of 40% of the diffuser length. The hub detachment seems to arise from a disturbance generated at the moving impeller hub/stationary diffuser wall interface. This hub separation extends to the volute and a high swirl flow zone is found at the volute, especially at the section near the tongue. Also, due to sudden expansion of the diffuser-volute interface, a high circulation region is found also at the shroud side. Because the fan was made of plexiglas, it was too difficult to make the cross section of the volute rounded. The diffuser hub separation is also seen by Kirtley and Beach [15] for NASA Lewis Low Speed Centrifugal Compressor. At off-design conditions, at a flow rate 150% of the design mass flow, Fig. 5 shows that, due to high flow momentum in the diffuser, the separation is very small near the hub, and that a high swirl flow zone occurs at the volute section near the tongue. This swirl flow zone is gradually attenuated from section B-B to section D-D. At flow rate 40% of the design mass flow, Fig. 6 shows a high separation region occurs at the beginning of the diffuser near the hub and that a massive recirculation zone is somewhat larger than the throughflow zone. This blockage near the hub deviates the flow towards the shroud to pass through a small area, which results in increasing the flow velocity near the shroud of the diffuser.

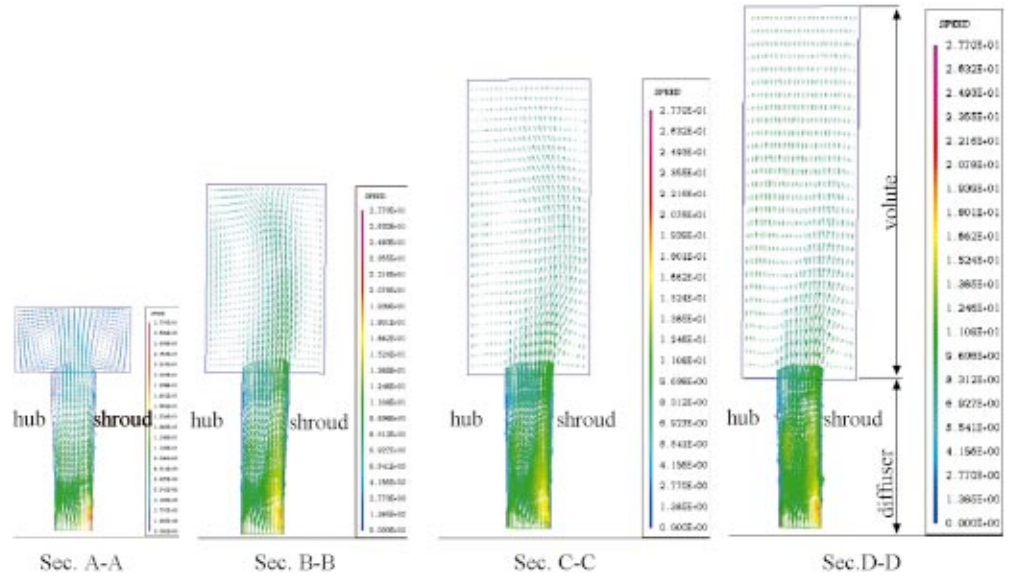

Fig. 5 Velocity vectors at 150% design flow rate for diffuser and volute at different sections

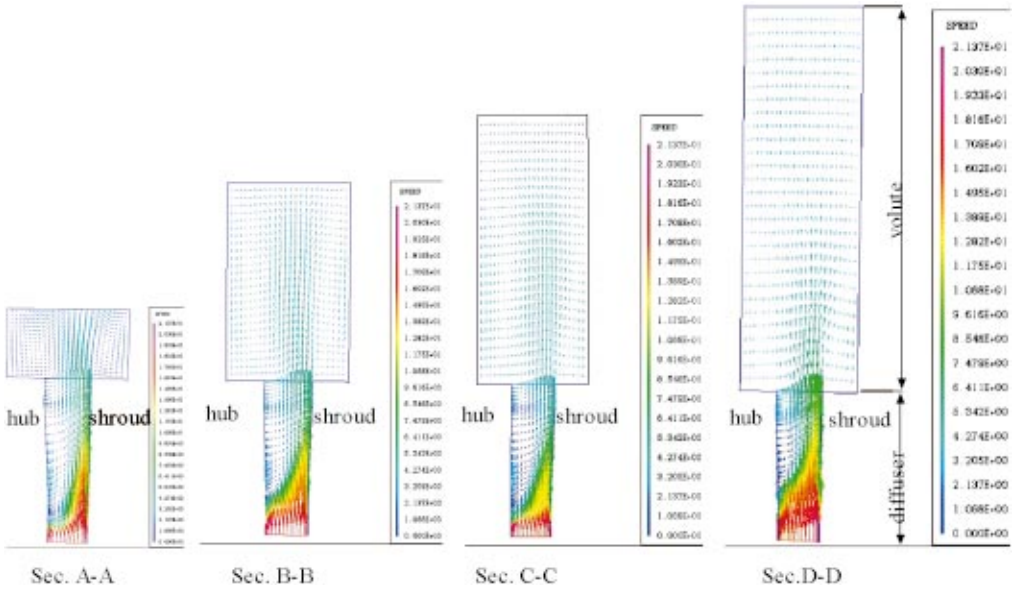

Fig. 6 Velocity vectors at 40% design flow rate for diffuser and volute at different sections

2 Transient Rotor-Stator-Volute Simulation. A huge amount of data has been obtained during a cycle of the transient simulation process. One cycle is divided into 20 timesteps; each timestep requires ten iterations and a converged solution is obtained after three cycles (where the initial guess for the transient simulation is taken as the converged solution of the frozen rotor simulation). Due to the large amount of data, all of the impeller positions could not be presented here; only one position (when the impeller blade matches the diffuser blade) is selected and presented for each case.

Figure 7 shows the instantaneous pressure field at (BEP) at midspan from the impeller inlet to the volute outlet. The potential effect, when the impeller trailing edge passes in front of the diffuser vane leading edge, is clearly visible. Pressure perturbations due to the vortex shedding behind the impeller blades can be observed also. In a small band around the vaneless space between the impeller blades and diffuser blade, complex pressure structures can be observed. These pressure structures are well correlated with the unsteady part of the relative velocity at the exit of the impeller. Outside this band, the pressure field is smoother and it can be observed that the pressure unsteadiness in the impeller is well synchronized. These global pressure variations are due to potential effects. It can also be noted that in the diffuser the pressure is changing with time only in the semi-vaneless space. Inside the diffuser and volute, the pressure variation is very small because the rotational speed of the impeller is very small.

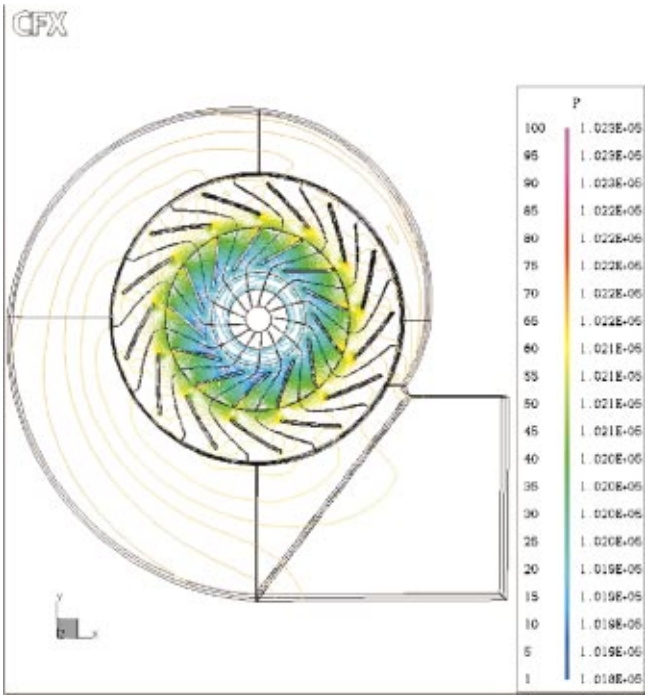

Fig. 7 The instantaneous pressure field at midspan

Since the computations are performed in a rotating frame in the impeller and in a fixed frame in the diffuser, it is natural to present the velocity field for both frames. Figure 8 shows the instantaneous relative velocity vectors in the impeller and the absolute one in the diffuser at the BEP at midspan. The evolution of the absolute velocity is viewed in a fixed frame. Conversely, the evolution of the relative velocity is viewed by an observer attached to the impeller. This gives a good overview of the rotor-stator-volute interaction mechanisms. Careful examination of velocity vectors behind the trailing edge of the impeller blade suggests vortex shedding. A low velocity region moves with the blade trailing edge in the vaneless space in the same direction of the diffuser blade. The flow in the vaneless space is very complex and this complicated flow pattern disappears beyond about 1.2 times radius of the impeller. Also, it is noted that a lower velocity region is found at the diffuser exit near the volute tongue.

3 Comparison between Experimental and Numerical Results at the Interaction Region of Impeller and Diffuser. The complexity of the impeller flow as well as the inhomogeneity of the impeller discharge flow and its interaction with the flow in the diffuser make it very difficult to bring together the whole field simulation with real flow measured by the PIV. So far, no one made a comparison between numerical and experimental unsteady flow of the whole machine because it is too complicated to model correctly and to measure experimentally in the interaction region between the impeller and the diffuser. However, some comparisons are presented here to see how well the present computation method can simulate the unsteady interaction and also to show the flow behaviors, which could not be obtained by PIV in some

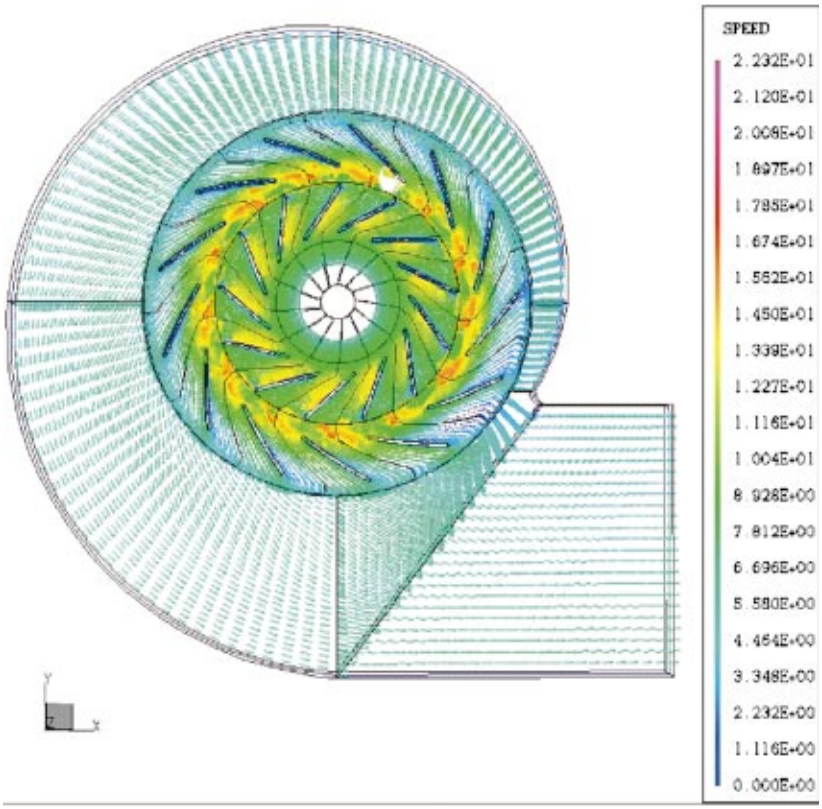

Fig. 8 The instantaneous velocity vectors at midspan

regions of the measurement area due to seeding problems or laser sheet accessing. Figures 9–11 show the comparison of the instantaneous absolute flow velocity vectors at medium flow rate at one relative position near the shroud, at midspan and near the hub, respectively. From a macroscopic point of view the agreement between experimental and numerical results is good in the sense that

1. The absolute flow velocity inside the impeller is higher than that inside the diffuser.
2. The absolute flow velocity near the shroud is a little higher than that at midspan and very small near the hub of the diffuser where a reverse flow zone pushes the flow towards the shroud.

From a microscopic point of view, it must be pointed out that there are some shortcomings of using PIV and computations. They are

1. There is a 2 mm clearance gap (which is relatively big) between impeller walls and diffuser walls along the whole circumference. This gap is a source of leakage and a highly three-dimensional flow with high axial flow velocity at the exit of the impeller along the span (from hub to shroud). The leakage of the flow with seeding in this region makes it too difficult to obtain the experimental results in this region. On the other hand, the present calculations did not consider the flow simulation in the clearance gap. The above two reasons may answer the question why the

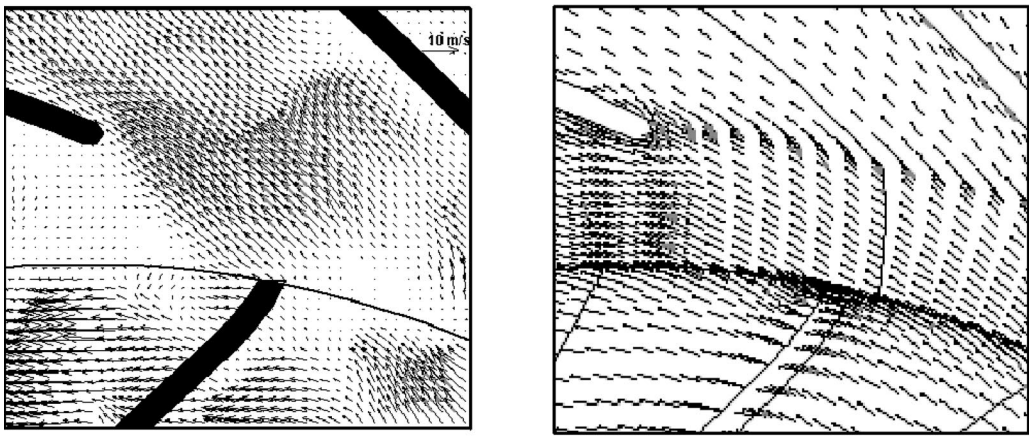

Fig. 9 Comparison of the instantaneous absolute flow velocity at design flow rate near the shroud

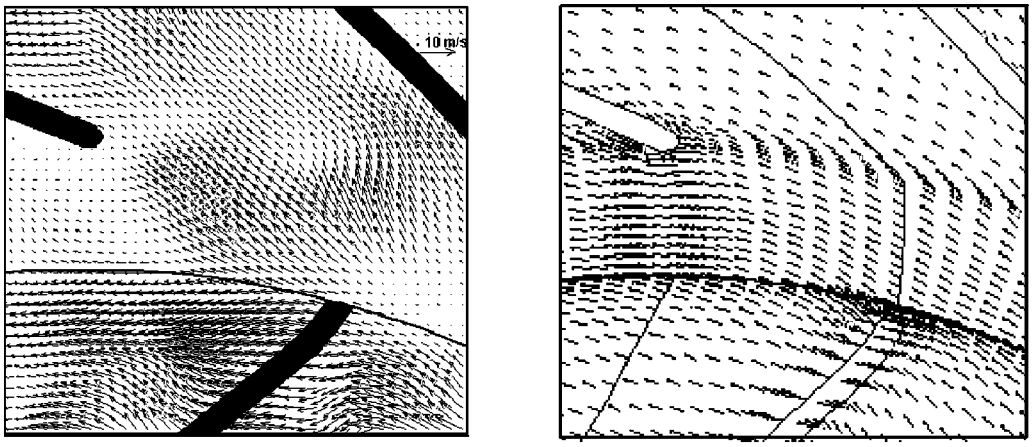

Experimental Numerical

Fig. 10 Comparison of the instantaneous absolute flow velocity at design flow rate at midspan

velocity at the exit of the impeller is low from experiment and high from numerical results.

2. The regions near walls and beside the leading edge of the diffuser vanes prevent PIV laser sheets from accessing and hence the data could not be obtained at these regions.

3. The instantaneous flow obtained from the computations is very smooth compared to the experimental results. This may be due to the turbulence model used, which is the standard K-ε model without any modifications (for example, the effect of curvature and rotation have not been taken into account). Another possible reason is that the real flow obtained by PIV is like a pulsating flow with unsteady inlet and outlet boundary conditions contrast to the steady state boundary conditions applied to the computations.

4 Performance Comparison. After applying the total pressure as inlet boundary conditions instead of applying inlet mass flow rate or inlet velocity, as mentioned in the boundary condition section, and applying the static pressure at the outlet, mass flow (or flow coefficient) rate is obtained. Using this flow coefficient the performance curve can be plotted as shown in Fig. 12. The discrepancy between the experimental and the numerical curves is due to the error in mass flow rate calculation. At design conditions ($\varphi = 0.07$), however, the discrepancy is less than 5%.

Conclusion

Unsteady flow simulations of the whole machine have been carried out by using the CFX-Tascflow code and the results are compared with the experimental results.

The following conclusions can be drawn from the present work.

1. A low velocity region behind the impeller blade is found at the suction side due to the formation of the wake at this region. A small vortex shedding can be observed and a highly distorted flow is seen at the vaneless space due to the interaction between the rotating blades and the stationary blades. Near the hub, the flow is much different from those of the other sections where the flow is highly unsteady and separated.

2. A massive recirculation zone is found near the hub and a throughflow zone near the shroud of the diffuser resulting from the inlet of the impeller. The detached flow at the diffuser extends to the volute. The transient simulation predicts a highly unsteady flow region in the vaneless space between the impeller and diffuser. The swirl flow zone in the volute is gradually attenuated from the section near the tongue to the outlet of the fan. Finally, the comparison between the measurements and the calculations showed that the rotor/stator model can predict the basic character-

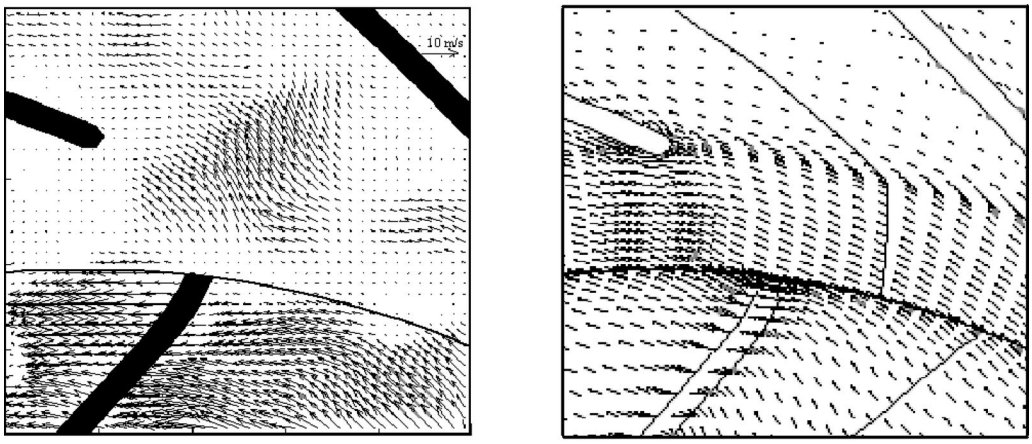

Experimental Numerical

Fig. 11 Comparison of the instantaneous absolute flow velocity at design flow rate near the hub

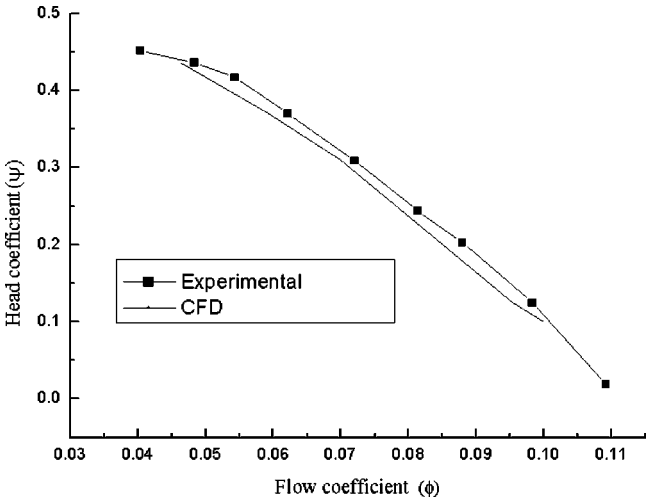

Fig. 12 Comparison between experimental and CFD results

istics of unsteady flow in centrifugal fan but still needs improvement to satisfy the true transient simulation for unsteady impeller diffuser interaction.

3. A good agreement is obtained between the experimental and CFD results for the performance.

Acknowledgment

The authors are grateful to the Brain-Korea 21 at KAIST for supporting this work.

Nomenclature

b = Impeller width
r_2 = Impeller radius
C_{mer} = Meridional velocity
C_{rad} = Radial component of velocity
C_{tan} = Tangential component of velocity
C_{ax} = Axial component of velocity
I = Streamwise direction
J = Circumferential direction
K = Spanwise direction
U_2 = Peripheral speed
PS = Pressure side
SS = Suction side
ϕ = Flow coefficient $= Q/(\pi r_2^2 U_2)$
ψ = Head coefficient $=$ Pstatic$/\rho U_2^2$

References

[1] Inoue, M., and Cumpsty, N. A., 1984, ''Experimental Study of Centrifugal Impeller Discharge Flow in Vaneless and Vaned Diffusers,'' ASME J. Eng. Gas Turbines Power, **106**, pp. 455–467.
[2] Sideris, M. T., and Van den Braembussche, R. A., 1987, ''Influence of a circumferential exit pressure distortion on the flow in an impeller and diffuser,'' ASME J. Turbomach., **109**, pp. 48–54.
[3] Arndt, N., Acosta, A. J., Brennen, C. E., and Caughey, T. K., 1989, ''Rotor-Stator Interaction in a Diffuser Pump,'' ASME J. Turbomach., **111**, pp. 213–221.
[4] Arndt, N., Acosta, A. J., Brennen, C. E., and Caughey, T. K., 1990, ''Experimental Investigation of Rotor-Stator Interaction in a Centrifugal Pump With Several Vaned Diffusers,'' ASME J. Turbomach., **112**, pp. 98–108.
[5] Paone, N., Riethmuller, M. L., and Van den Braembussche, R. A., 1989, ''Experimental Investigation of the Flow in the Vaneless Diffuser of a Centrifugal Pump by Particle Image Displacement Velocimetry'' Exp. Fluids, **7**, pp. 371–378.
[6] Hillewaert, K., and Van den Braembussche, R. A., 1999, ''Numerical Simulation of Impeller-Volute Interaction in Centrifugal Compressor,'' ASME J. Turbomach., **121**, pp. 603–608.
[7] Meakhail, T., Zhang, L., Du, Z. H., Chen, H. P., and Jansen, W., 2001, ''The Application of PIV in the Study of Impeller Diffuser Interaction in Centrifugal Fan. Part I—Impeller-Vaneless Diffuser Interaction,'' *Proceedings of The ASME Fluid Engineering Division*-IMECE2001/FED-24952 November 11–16, 2001, New York, USA.
[8] Meakhail, T., Zhang, L., Du, Z. H., Chen, H. P., and Jansen, W., 2001, ''The Application of PIV in the Study of Impeller Diffuser Interaction in Centrifugal Fan. Part II—Impeller-Vaned Diffuser Interaction,'' *Proceedings of The ASME Fluid Engineering Division*- IMECE2001/FED-24953 November 11–16, 2001, New York, USA.
[9] ASC, 1999, ''CFX-TASCflow Documentation Version 2.9.0,'' Advanced Scientific Computing, Ltd., Waterloo, Ontario, Canada.
[10] Gernot, E., Peter, D., Krain, H., Hartwig, P., Franz, A. R., and Karl, H. R., 1998, ''Analysis of the Transonic Flow at the Inlet of a High Pressure Ratio Centrifugal Impeller,'' ASME paper no. 98-GT-24.
[11] Peter, D., and Donald, H. W., 1995, ''Numerical Transonic Flow Field Predictions for NASA Compressor Rotor 37,'' ASME paper no. 95-GT-326.
[12] Mihael, S., Matija, T., and Dusan, F., 1998, ''Characteristics of One Stage Radial Centrifugal Turbine,'' ASME paper no. 98-GT-494.
[13] ASC, 1999, ''CFX-Turbogrid Documentation Version 1.4,'' Advanced Scientific Computing, Ltd., Waterloo, Ontario, Canada.
[14] Eckardt, D., 1976, ''Detailed Flow Investigations Within a High Speed Centrifugal compressor Impeller,'' ASME J. Fluids Eng., **98**, pp. 390–402.
[15] Kirtley, K. R., and Beach, T. A., 1992, ''Deterministic Blade Row Interactions in a Centrifugal Compressor Stage'' ASME J. Turbomach., **114**, pp. 304–311.
[16] Hamkins, C. P., and Flack, R. D., 1987, ''Laser Velocimeter Measurements in Shrouded and Unshrouded Radial Flow Pump Impellers'' ASME J. Turbomach., **109**, pp. 70–76.
[17] Krain, H., and Hoffman, W., 1989, ''Verification of an Impeller Design by Laser Measurements and 3D-Viscus Flow Calculations'' ASME paper no. ASME 89-GT-159.